ACS APPLIED MATERIALS & INTERFACES

Research Article

www.acsami.org

Electrodynamically Sprayed Thin Films of Aqueous Dispersible Graphene Nanosheets: Highly Efficient Cathodes for Dye-Sensitized Solar Cells

Sung-Yeon Jang,*[,†] Young-Gon Kim,[‡] Dong Young Kim,[‡] Hong-Gon Kim,[§] and Seong Mu Jo[‡]

[†]Department of Chemistry, Kookmin University, 861-1 Jeongneung-dong, Seong-buk, Seoul, Korea.

[‡]Nanohybrids Center and [§]Solar Cells Center, Korea Institute of Science and Technology, 39-1 Hawolgok-dong, Seong-buk, Seoul, Korea

Supporting Information

ABSTRACT: Highly efficient cathodes for dye-sensitized solar cells (DSSCs) were developed using thin films of graphene nanosheets (GNS), which were fabricated by the electrospray method (e-spray) using aqueous dispersions of chemically driven GNS. The e-sprayed GNS films had the appropriate properties to be an efficient counter electrode (CE) for DSSCs; sufficient electrocatalytic activity for I^-/I_3^- redox couples and low charge transfer resistance (R_{CT}) at the CE/electrolyte interface as characterized by cyclic voltammetry and electrochemical impedance analysis. The performance of the GNS film based CEs was optimized by manipulating the density of surface chemical functional groups and plane conjugation of GNS via post thermal annealing (TA). Upon TA, the oxygen-containing surface functional groups, which have been shown to improve electrocatalytic activity of carbon based materials, were significantly reduced, while the electrical conductivity was enhanced by ~40 times. The improvement of electrocatalytic activity and fill factor (FF) with reduced R_{CT} of DSSCs after TA was primarily attributed to the increased charge transport within the GNS films, while the chemically prepared GNS typically contained sufficient defects, edges and surface functional groups for electrocatalysis. The performance of the DSSCs using our GNS-CEs was nearly identical (>95%) to the DSSCs using the state-of-the-art CE, thermolytically prepared Pt crystals. Our e-sprayed GNS-CE based DSSCs had a higher FF (69.7%) and cell efficiency (6.93%) when compared previously reported graphene based CEs for DSSCs, demonstrating the outstanding properties of graphene as the electrodes in electrochemical devices.

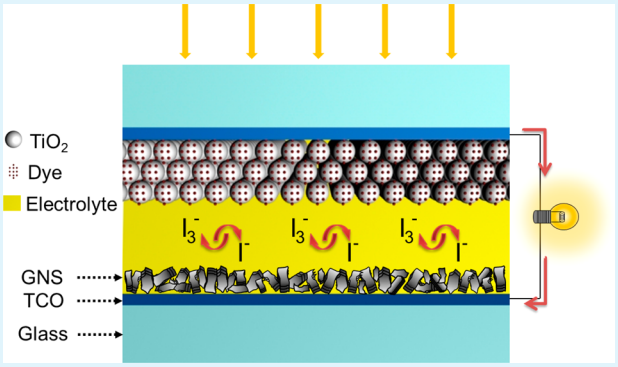

KEYWORDS: *graphene, dye-sensitized solar cell, counter electrode, thermal annealing, electrocatalytic activity*

INTRODUCTION

Graphene-based materials have received much attention as emerging materials because of their atypical electronic, optical, and thermal properties.[1,2] Because of the properties of graphene, including extremely high carrier mobility and ambipolar characteristics,[3−7] high electrical conductivity when used as thin layers,[8,9] and sensitivity in detecting environmental change, these materials hold great promise for use in field effect transistors, transparent conducting electrodes, and chemical[10,11] and biological sensors.[12−14] Their large surface area enhanced the mechanical properties of composites when used as a nanofiller.[15,16] Graphene can be prepared by various routes such as mechanical cleavage of graphite,[3] high temperature epitaxial growth on SiC[17,18] or ruthenium,[19] and chemical vapor deposition on nickel[20] or copper.[21] Among these approaches, chemical preparation methods, which typically involve reducing suspensions of the precursor oxides in solution, have several advantages including large-scale production, reasonable processablility, and manipulation of functionalization.[22−25]

The potential of using graphene-based materials for electrochemical devices has been widely investigated because of the electrocatalytic activity and the high surface area of these materials. Reports on the applications of these materials to fabricate electrochemical energy devices such as fuel cells,[26−28] supercapacitor,[29−31] and lithium rechargeable battery[32−34] have been grown recently. Studies to improve the performance of devices and expand the range of applications via optimizing the properties of graphene materials are ongoing.

Dye-sensitized solar cells (DSSCs) are widely used solar conversion devices that have been studied for more than 20 years. Their simple process and low cost with relatively high energy conversion efficiency have drawn the attention of researchers and industries.[35] In DSSCs, the counter electrode (CE) is one of the most crucial components dictating the

Received: April 5, 2012
Accepted: June 24, 2012
Published: June 24, 2012

 © 2012 American Chemical Society

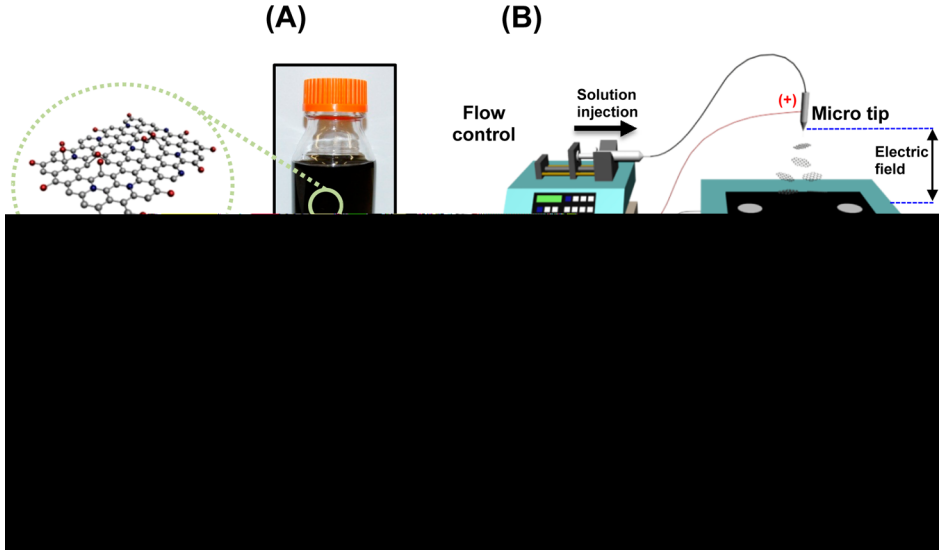

Figure 1. Process used to fabricate the GNS thin film CEs. (A) An image of the aqueous GNS solution. The concentration of the solution is 0.3 $mgml^{-1}$. (B) Schematic diagram of the e-spray technique used for GNS thin film fabrication. (C) An image of the e-sprayed GNS thin film CE (~200 nm thick). (D, E) SEM images of the e-spayed GNS-based CEs; as (D) e-sprayed, and (E) after TA. The scale bars at the up-right position of images indicate 500 nm.

power conversion efficiency (PCE) because the electrons that are supplied through the CEs have to be sufficient to reduce the redox mediators (typically I^-/I_3^-) that were oxidized for dye regeneration. For efficient CEs, high electrocatalytic activity for the redox couples and enhanced electrical conductivity to transport charges are required. Platinum has been used to fulfill these requirements, however it is relative expensive. Nanocarbons have widely been suggested as cheap alternatives to Pt and can fulfill the requirements to produce effective CEs with good chemical stability. Conventional carbon based materials and nanocarbons including carbon nanotubes (CNTs) and fullerenes have been used for CE, indicating that these material may be used in the development of next generation DSSC−CEs.[36−42] Recently, CEs using thin films of water-soluble CNTs that were prepared by the electro-spray (e-spray) method were reported by our group.[42] The performance of DSSCs using our MWCNT thin films CE was ~85% of the performance of DSSCs fabricated using Pt based CEs (Pt-CEs). Furthermore, their low temperature processing capability indicated that they may be used to fabricate plastic DSSCs.

Despite the growth of research on DSSC−CEs using nanostructured carbon materials, the applicability of graphene-based materials as the CEs has been elusive. There have been a few reports on the application of graphene based materials as CEs, which were prepared by drop/spin-casting commercial graphene nanoplatelets[43,44] or electrophoretically depositing graphene nanosheets.[45] However, the results have not been successful to demonstrate the preferential properties of graphene materials in CE applications and research in this area is still in progress.

In this study, highly efficient thin film CEs for DSSCs were developed using chemically driven aqueous dispersible graphene nanosheets (GNS). The GNS thin films were prepared by e-spray method from its aqueous solution. The essential factors that influence the performance of CEs, such as electrocatalytic activity, charge transfer resistance, and electrical conductivity were investigated in terms of the evolution of surface chemical structures of GNS. The efficiency of GNS thin film CEs (GNS-CE) was dramatically improved by post thermal annealing (TA), which further reduces the oxygen concentration on the edges of GNS. The performance of the optimized e-sprayed GNS-CEs was nearly identical to the performance of the state-of-the-art CE material, thermolytically prepared Pt. The electrocatalytic effect of the redox mediators and reduced R_{CT} at the CE/electrolyte interface of GNS-CEs were investigated using cyclic voltammetry (CV) and electrochemical impedance spectroscopy (EIS), respectively. The PCE of the DSSCs using our GNS film CE (DSSC-GNS) was 6.93%, whereas that of DSSCs using Pt-CE (DSSC-Pt) was 7.23%. This cell efficiency was substantially higher than other reported values (2.2−5.6%) from cells that used other graphene materials as CEs.[43−46] Notably, the fill factor (FF) of our DSSC-GNS was extraordinarily high (69.7%), which is the first report of a fill factor value higher than the reference DSSC-Pt (68.1%). Furthermore, our GNS-CE possessed unique advantages such as low thickness (~200 nm) and materials consumption, and the use of an aqueous solution.

RESULTS AND DISCUSSION

The GNSs used in this study were prepared by the aqueous phase chemical reduction of graphene oxide (GO) following the synthetic route by Li et al[23] with minor modifications. Briefly, graphite was chemically oxidized using the modified Hummer method[22,47] to obtain an aqueous dispersion of graphite oxide. Exfoliation of graphite oxide under ultrasonication yielded well-dispersed GO colloids. The aqueous dispersion of GNSs was formed by reduction of the GO suspension using hydrazine hydrate followed by dialysis. During this process, a mild basic condition (pH ~9) was maintained to obtain well dispersed GNS solutions. This was needed because the repulsion among the negative charges on the perimeter of the GNSs helps dissolution. Well-dispersed aqueous GNS solutions were successfully prepared at a concentration of ~0.3 mg mL in deionized (DI) water. The zeta potential values of the GNS solutions were −35 to −40 mV, ensuring the stability of the solution that stems from electrostatic repulsion of the ionized residual functional groups.[23,48] The preparation of stable GNS dispersions is essential issue for any kind of film

fabrication method. The improved surface area and porosity inside the GNS films with reduced aggregation as well as high film surface quality can be readily obtained when well-dispersed stable solutions are used during the film fabrication process.

The thin films of GNS were prepared on a fluorine-doped tin oxide (FTO) coated glass plate using the e-spray method (Figure 1B). The e-spray is a gentle and efficient deposition method that produces low thickness variation and lower material consumption.[49,50] A good surface morphology and enhanced adhesion to the substrates have been observed in e-sprayed CNT films that were subsequently used as electrodes for electrochemical devices.[42,49] In our earlier study, high performance CE for DSSCs were developed using the e-sprayed thin films of water-soluble MWCNTs. This binder-free, room-temperature process produced high-quality CNT-based electrodes from their stable solutions.[42] Our aqueous GNS solution was stable enough to use the e-spray method for film deposition. The deposition could be continuously performed >24 h without clogging the nozzle, and the resulting film thickness was proportional to the deposition time. Figure 1A shows the well-dispersed GNS solution (0.16 $mgml^{-1}$) in a DI-water/ethanol (6/4), which was used for the e-spray process. The apparent stability and the zeta-potential values were nearly identical to the prepared GNS aqueous solution. The GNS-CEs deposited on the FTO/glass displayed good uniformity (Figure 1C). As shown in the scanning electron microscopy (SEM) images in Figure 1D,E, the e-sprayed GNS layer had an open and layered morphology and noticeable macro-aggregation events were not observed, indicating that the e-spray method is an effective technique to prepare GNS films. The specific surface area and pore volume of the films, which were analyzed using the Brunauer–Emmett–Teller (BET) method, were 276 $m^2\ g^{-1}$ and 0.19 $cm^3\ g^{-1}$ respectively.

DSSCs were fabricated using the GNS thin film as CEs. The photoanodes were prepared by doctor blading commercial TiO_2 nanoparticle pastes (Nanoxide D, Solaronix) on FTO/glass followed by sintering at 500 °C for 30 min. The N719 (Solaronix) sensitizer was loaded on the surface of the TiO_2 nanoparticles by immersing the photoanodes into a dilute alcoholic solution and incubating overnight. Finally, a conventional organic liquid electrolyte was injected into the preassembled cells to complete the sandwich type cells (details for cell fabrication are in the Experimental Section). Figure 2 shows the structure of DSSCs using our GNS-CEs. The Pt-CEs were prepared using a thermal reduction method, where a Pt precursor ($H_2PtCl_6{\cdot}H_2O$) was drop casted on the FTO/glass followed by thermal treatment at 450 °C for 20 min. This method is known to yield highly crystalline Pt layers that perform the best as CEs.[51−53] Figure 3 shows the J–V characteristics of the DSSC-GNSs and a DSSC-Pt under 1 sun illumination (100 mW cm^{-2}, AM 1.5G). The PCE of the DSSC-GNS using the as-sprayed films was 5.45% (with FF of 57.2%) while the PCE of the DSSC-Pt was 7.23% (with FF of 68.1%), indicating the GNSs had decent activity (albeit lower than Pt) as a CE. When the GNS-CEs were further treated by post TA at 400 °C for 4 h under argon, the cell efficiency was drastically improved. The PCE of the DSSC-GNSs after TA reached 6.93% with an open circuit voltage (V_{OC}), short circuit current density (J_{SC}), and FF of 812 mV, 12.22 mA, and 69.7%, respectively. This was a remarkable improvement and the cell efficiency was nearly identical to the DSSC-Pt. The dramatic improvement in performance was attributed to an improved FF upon post TA, while the other parameters were relatively unaffected. The values from the J–V characteristic curves in Figure 3 are listed in Table 1. To the best of our knowledge, this is the first report where graphene-based CEs had a higher FF than Pt-CEs. Because the FF is directly related to the internal series resistance (R_S), the DSSCs were analyzed by electrochemical impendence spectroscopy (EIS).

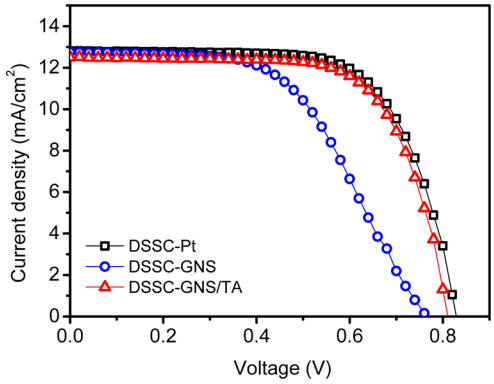

Figure 3. J–V characteristics of DSSCs using GNS- and Pt-CEs under simulated AM 1.5G one sun condition; as e-sprayed GNS-CE, blue circles; GNS-CE after TA, red triangles; and Pt-CE, black square. The thickness of TiO_2 photoanodes was ~8 μm.

Table 1. J–V Analysis Results of DSSCs

device	V_{OC} (V)	J_{SC} (mA/cm^2)	FF (%)	PCE (%)
DSSC-Pt	0.828	12.80	68.1	7.23
DSSC-GNS	0.752	12.66	57.2	5.45
DSSC-GNS/TA	0.812	12.22	69.7	6.93

EIS characterization can provide useful information on the catalytic performance of CEs in regards to the reduction of I_3^-.[51,54,55] Figure 4 shows the Nyquist plots and the equivalent circuit diagram of the DSSCs. The high frequency (leftmost) semicircle indicates the electrochemical charge transfer resistance at the CE/electrolyte interface (R_{CT}) while the combined semicircle in the mid-frequency and low frequency indicates impedance by transport and recombination competition at the TiO_2/dye/electrolyte interface (R_{AN}), and Nernst diffusion limited impedance of the I^-/I_3^- redox species in the electrolyte (R_D) (also refer the inset graph of Figure 4).[39,56,57] The R_{CT} at the CE/electrolyte interface can be obtained from the real component (Z′) values. The R_{CT} of the GNS-CEs after

Figure 2. Structure of the DSSC using GNS films as a counter electrode. (TCO: transparent conducting electrode).

dx.doi.org/10.1021/am3005913 | ACS Appl. Mater. Interfaces 2012, 4, 3500–3507

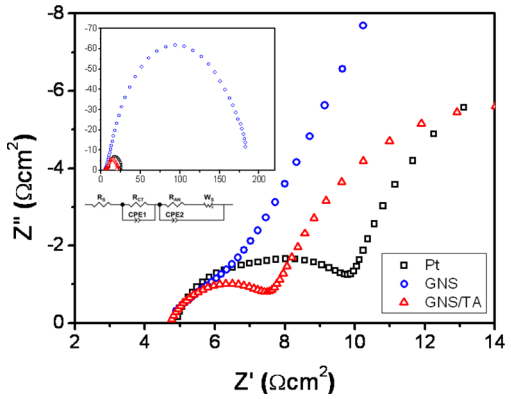

Figure 4. Nyquist plots of DSSCs using GNS- and Pt-CEs at the open circuit condition under simulated AM 1.5G one sun light; as e-sprayed GNS-CE, blue circle; GNS-CE after TA, red triangles; and Pt-CE, black square. Inset shows the full-range plot. The circuit diagram used for simulation is inserted.

TA was lower (2.37 Ωcm^2) than that of Pt-CE (4.07 Ωcm^2). The charge transfer at the GNS-CE/electrolyte interface was dramatically improved by post TA, and even superior to Pt-CE. Note that the high-frequency semicircle of the GNS-CE without TA was too large to be discernible from the lower-frequency semicircle as indicated in Figure 4. It is worth emphasizing that the FF of the DSSC-GNS (after post TA) was higher than (if not, comparable to) that of DSSC-Pt, and the GNS thin film performed well even at a very low thickness (100−200 nm).

To further investigate the electrocatalytic properties of GNS-CEs and the effects of TA on the electrocatalysis of the I^-/I_3^- redox couple, cyclic voltammetry (CV) analysis was performed (Figure 5). In the CV analysis, the CEs used for the DSSCs (e-

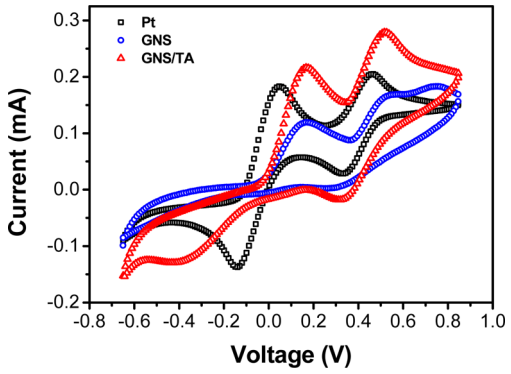

Figure 5. Cyclovoltammograms of the GNS- and Pt-CEs for the Redox reaction of I_2/I_3^- and I^-/I_3^-. The scan rate was 10 mVs^{-1}. A Ag/Ag^+ reference electrode (0.01 M $AgNO_3$ in acetonitrile) was used.

sprayed GNS films and thermolytically prepared Pt deposited FTO) were used as the working electrodes. The deposition area for all the CEs was ∼0.4 cm^2 and the thickness of the GNS films was ∼200 nm. It is known that the redox pair at the more positive potentials is due to $I_3^- + 2e^- = 3I^-$, whereas the redox pair at the more negative potentials is the redox pair of $3I_2 + 2e^- = 2I_3^-$.[53,58] The left pair of the peaks, which indicates the I^-/I_3^- redox process, is of interest for the performance of CEs. The GNS films showed the characteristic CV curves of I^-/I_3^- redox pairs, which is the prerequisite for a DSSC-CE. It is worth noting that the CVs of FTO did not display the characteristic peaks of the redox process; thus the contribution of any exposed FTO is negligible. The peak to peak separation (E_{pp}) of the left pair of the as prepared GNS films was larger than that of Pt-CEs, which occurred because the redox reaction rate of the Pt was faster than GNS. The peak exchange current (I_p) of the as e-sprayed GNS-CEs was also lower than Pt-CEs, indicating that the I_3^- was reduced less at the GNS-CEs. However, the I_p values of the e-sprayed GNS increased dramatically up to values comparable to Pt after TA treatment, although the E_{pp} of the GNS-CEs was nearly unchanged (refer the CV curves for GNS and GNS/TA in Figure 5). This result indicates that the rate of electocatalysis in GNS-CE was unchanged after TA; however, more redox reactions occurred after TA and comparable to the Pt-CE. Since the specific surface area of the GNS films was unchanged by TA, the improved electrocatalysis upon TA of the e-sprayed GNS-CEs was probably due to changes in other properties of GNSs. The effect of TA on the chemical structure and the electrical conductivity of the GNS will be discussed in the following sections.

The chemical structure of the GNS films was characterized using X-ray photoelectron spectroscopy (XPS) and Raman spectroscopy. The C_{1s} XPS spectrum of the GNS (Figure 6A) clearly indicated the formation of graphene based materials including some degree of oxidation due to incomplete restoration by chemical reduction. Functional groups corresponding to sp^2 C−C (∼284.6 eV) were observed in the basal plan of GNS, C−O (∼286.5 eV), C═O (∼288.7 eV), C═O−O (∼289.1 eV).[22,59] As a result of chemical reduction using hydrazine, there was an additional component at ∼285.9 eV corresponding to C−N bonding.[22,60] The peak intensities of the oxygen functionalities were significantly reduced after TA as indicated in Figure 6B and C. The C−C/C═O peak intensity ratio of GNS increased by ∼3 times after TA (11.0 for the as prepared GNS and 31.9 for TA treated GNS), whereas the C−C/C−O peak intensity ratio increased by only 19%. These results indicate that the carbonyl groups were removed by the TA, which are not efficiently reduced by chemical reducing agents.[48,61] The C/O ratio determined by the XPS analysis were 5.66 for the as prepared GNS and 8.65 for the GNS after TA. Structural changes in the GNS were also characterized by Raman spectroscopy based on the two characteristic absorption bands; the G band at around 1580 cm^{-1} and the D band at 1350 cm^{-1}. The G band is associated with bond stretching of the sp^2 carbon pairs in both rings and chains, whereas the D band is due to the breathing mode of aromatic rings with dangling bonds in plane terminations.[22] The D/G intensity ratio is a typical criterion used to evaluate the crystal structure of graphene-based materials. The D/G ratio of the as prepared GNS (1.06) was in the typical range of chemically prepared graphene materials,[22,61] and was reduced upon TA (0.97) (refer to Figure S1 in the Supporting Information). This indicates that either a decrease in the defects sites or increase in the average size of the sp^2 crystalline domain in the as-prepared GNS occurred after TA at 400 °C.

The effect of chemical structure evolution of GNSs on electrical conductivity was investigated by four points probe measurements of the GNS thin films on glass substrates. The electrical conductivity of the as-sprayed GNS films was 150 S/m, while that of the same GNS films after TA was 6000 S/m. The thickness of the GNS films was ∼200 nm, which was determined using a surface profiler (TENCOR P-10). This conductivity values was consistent over a range of film

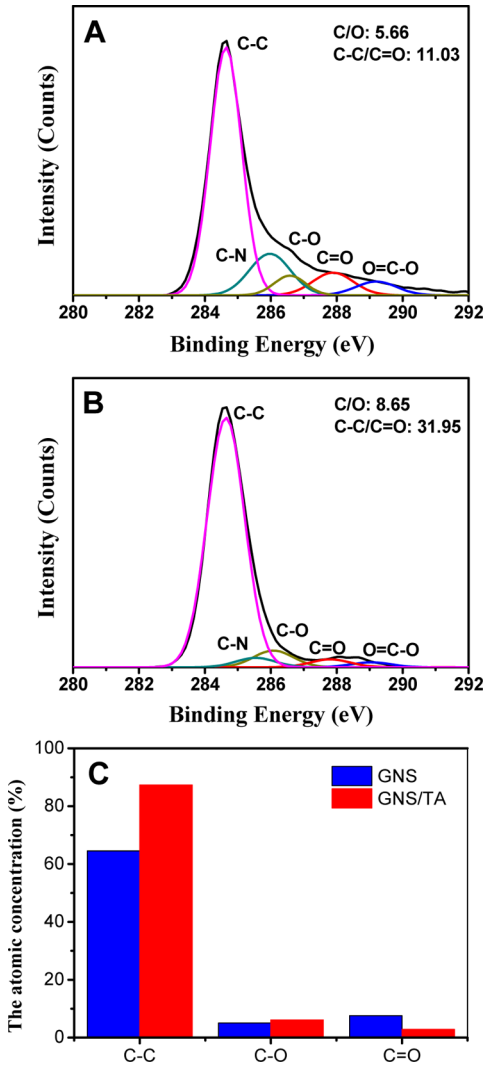

Figure 6. XPS spectra (C1s) of e-sprayed GNS films; (A) as e-sprayed film and (B) TA-treated film. (C)Atomic concentration of C−C, C−O, and C═O for GNSs by integration of the XPS peaks.

thicknesses (100 nm ∼1 μm). Since there was no detectable thickness change during TA, the enhanced electrical conductivity upon TA can be attributed to changes in the chemical structures observed by the XPS and Raman analysis (Figure 6 and Figure S1 in the Supporting Information). The removal of oxygen-containing functional groups, which can act as defects of charge transport, by TA was responsible for the increased conductivity, which improves intersheet interactions.[44,62]

To be an efficient CE material for DSSCs, various factors need to be considered; (i) the sufficient electrocatalytic activity for the I^-/I_3^- redox reaction is required, (ii) enhanced surface area can increase the sites for the redox reaction, (iii) high electrical conductivity can facilitate charge transport during the reaction, and (iv) a lower charge transfer resistance between CE and the electrolytes is preferred. In the case of graphene-based materials, their high surface area is an intrinsically favored property. However, perfect graphene has not been considered as optimal candidate for a CE material because of the lack of available active sites for I^-/I_3^- electrocatalysis. It has been suggested that the active sites of the carbonaceous electrode materials are the defects and oxygen-containing surface functional groups, which are located at crystal edges of graphite and the activity of basal-plane graphite is low.[39,52,63,64] Thus, the chemically prepared GNSs possess another beneficial property for the electrocatalysis aside from their improved processability for electrode fabrication. However, despite the additional enhancement of catalytic activity and surface area, excessive functionalization of carbon materials deteriorates their electrical properties. In the early stage of research in this field, highly functionalized carbon based materials such as activated carbon (AC) were often used as a CE of DSSC.[52] Although AC had a high surface area and oxygen-containing functional groups, the efficiency of AC based CEs was low because of their poor electrical conductivity.[36] Mixing AC with conductive carbon enhanced the conductivity to some extend; however, this increment was not sufficient to be an efficient CEs. Even for graphene-based electrodes, excess conductive additives (binders) have often been used to enhance their electrical conductivity.[46,65] In the GNS, the density of functional groups and defects influence both the electrocatalytic activity and the electrical conductivity in an opposite manner, thus it is crucial to strategically address this issue to optimize the performance of the CEs.

Recently, Roy-Mayhew et al. reported the successful application of commercially available thermally exfoliated functionalized graphene sheets (FGS, Vor-x BK86 from Vorbeck Materials) as a CE for DSSCs. Using different grades of FGS, they observed that the FGS showed sufficient electrocatalytic activity when the C/O ratio was <13, while the electrical conductivity was inadequate when the C/O ratio was much less than 7. However, the thickness and electrical conductivity of their drop-casted polymer binder mixed FGS films were not clearly discussed in this previous study. Typically, chemically prepared GNS contains oxidic functional groups and their density is determined by the structure of their oxidized-state precursors and the reduction condition. Our GNS also contained some functional groups, just as in other chemically reduced graphene materials. The C/O ratio of the as prepared GNS films by chemical reduction was 5.66, which increased to 8.65 after TA. This result is in a good agreement with the values reported by Roy-Mayhew et al. As indicated in the CV curves in Figure 5, the shape and redox peak positions of the two GNS films (before and after post TA treatment) were similar, indicating the electrocatalytic activity of the two films are nearly identical. However, the I^-/I_3^- electrocatalysis peak currents of the GNS films after TA was much higher than that of the as-sprayed films. We attribute this majorly to the ∼40 times higher electrical conductivity of TA treated GNS films because the specific surface area of GNS films did not change considerably after TA. From the XPS results (Figure 6), the major functional groups that diminished after TA were C═O and O═C−O. This fact suggests that the removal of carbonyl or carboxylic groups, which are known to be present at the perimeter of the GNS, was responsible for the enhanced charge transport. This finding is in agreement with a similar study, where the electrical conductivity was shown to be enhanced by the removal of carboxylic acid group through thermal treatment. When the thermally treated graphene-based material was used in a supercapacitor,[66] the power density of the supercapacitor was shown to be significantly enhanced because of a reduction in series resistance.

We have recently developed high efficiency e-sprayed MWCNT thin film based CEs in which the thickness was >10 times less than previously reported CNT based CEs. The well exfoliated MWCNTs prepared by the e-spray method from

soluble CNT solutions without using any binder material resulted in good electrocatalytic activity. In this previous report, the PCE of the cells using MWCNT was ~85% of the cells using Pt-CE at a CNT film thickness of ~1 μm. The GNS-CEs in this study exhibited superior performance (>95% of PCE compared to DSSC-Pt) at substantially lower film thickness (<200 nm). This result indicates that the GNS films are an excellent material for CE with good electrocatalytic activity, higher surface area, and sufficient electrical conductivity when coupled using an efficient binder free fabrication method.

CONCLUSIONS

In summary, high efficiency thin film CEs for DSSCs were developed using chemically driven aqueous dispersible GNS that were coupled with the e-spray method. The performance of the e-sprayed GNS film CEs was optimized by manipulating the density of surface chemical functional groups and plane conjugation of GNS *via* chemical reduction and post TA treatment. After TA, the electrocatalytic activity of GNS-CE improved, although the number of catalytic surface functional groups was reduced. After TA, the electrical conductivity increased by ~40 times, which was the reason for the increased catalytic activity as well as the boosted FF and reduced R_{CT} of the corresponding cells. The performance of the e-sprayed GNS-CEs was identical to the state-of-the-art CE material, a thermolytically prepared Pt. The PCE of the DSSCs using our e-sprayed GNS-CE (6.93%) was substantially higher than other reported values (2.2–5.6%), while that of DSSCs using Pt-CE was 7.23%. Notably, the FF of our DSSC-GNS was extraordinarily high (69.7%). This is the first study where a higher FF value than the reference DSSC-Pt (68.1%) has been reported. Furthermore, our GNS-CEs possessed many unique advantages such as ultrathin (~ 200 nm), low materials consumption, and the use of an environmentally benign solution. These combined results indicate that the GNS would be an ideal material for use as a DSSC-CE. Applications of the e-sprayed GNS films for other electrochemical devices are currently being examined by our group.

EXPERIMENTAL SECTION

Preparation of Aqueous Dispersion of GNS. The graphite oxides was synthesized by the Hummer's method using graphite powder (Aldrich, <20 μm) with slight modifications.[47] Ultrasonication of graphite oxide (75 mg in 250 mL of H_2O) yielded an aqueous solution of GO. After 1 day of sedimentation, the GO solution was decanted for the GNS preparation. For GNS preparation, 400 uL of NH_3 solution (JUNSEI, ~ 30%) and 225 mg of hydrazine hydrate (35 wt % solution in water, Aldrich) were added to the aqueous solution of GO. The solution was covered with mineral oil (Aldrich) and heated at 95 °C for 1 h to complete the reduction of GO to GNS. Finally the hydrazine was removed from the GNS solution by dialysis (~7 days), yielding a stable aqueous GNS solution.

Preparation of GNS-CE. 0.1–0.3 mg mL^{-1} aqueous GNS solution (DI-water/EtOH, 6:4) was used for the e-sprayed process. The fluorine-doped tin oxide (FTO) glass (TEC-8, Pilkington) was drilled using a diamond tipped-micro drill, washed with 0.1 M HCl solution in ethanol, and then cleaned in a bath-sonicator containing water/EtOH for 15 min. A drilled FTO glass was placed on the grounded *x*, *y*-axis motion controlled e-spray system, whereas the GNS solution was loaded into a plastic syringe and the flow rate was controlled by a syringe pump (KD Scientific Model 220). The injection rate through the micro tip was 10–40 μL min^{-1}. An electric field of 1–2 kV cm^{-1} was applied between the FTO glass and the micro tip using a high voltage power supply (BERTAN SERIES 205B). For TA, the e-sprayed GNS films were heated in a furnace at 400 °C for 4 h under argon atmosphere.

DSSC Fabrication. Pt-CEs were prepared by drop casting of 5 mM H_2PtCl_6 (Aldrich) in isopropyl alcohol onto the washed FTO glasses and then sintered at 400 °C for 20 min under air condition. The TiO_2 nanoparticle-based photoanodes were prepared onto FTO/glass by the simple doctor-blade method using a commercial TiO_2 colloidal paste (Nanoide-D, Solaronix), and then sintered at 500 °C for 20 min in air condition. The prepared photoanodes were immersed in an anhydrous ethanol solution containing 3×10^{-4} M of purified cis-bis(isothiocyanato)bis(2,2′-bipyridyl-4,4′-dicarboxylato)ruthenium(II)-bis-tetrabutylammonium (N719 dye, Solaronix) and kept at room temperature for 20–24 hs. The dye adsorbed TiO_2 photoanodes were assembled with either GNS-CEs or Pt-CEs using a thermal adhesive film (25 μm thick Surlyn, Dupont) as a spacer to produce a sandwich-type cell. The liquid electrolyte consisting of 0.65 M 1-butyl-3-methylimidazolium iodide (BMII), 0.5 M 4-*tert*-butylpyridine (TBP), 0.03 M iodine (I_2) and 0.05 M guanidiniumthiocyanate (GSCN) in a mixture of acetonitrile and valeronitrile (85:15, v/v) was injected through a drilled hole on the CE side. The holes were sealed with cover glass using Surlyn.

Characterization. The morphology of the GNS-CEs was investigated using field emission scanning electron microscopy (FE-SEM, Hitachi S-4100) and high resolution transmission electron microscopy (HR-TEM, TECNAI G2). X-ray diffraction (XRD) measurements were carried out at room temperature using an X-ray diffractometry system (Bruker, D8 DISCOVER). The chemical structures of GNS were characterized using X-ray photoelectron spectroscopy (XPS) (ULVAC-PHI) and Raman spectroscopy (LabRam HR Raman system). The electrical conductivity was measured using a microvoltmeter (MCP-T610, Mitsubishi Chemical) in a four-probe setup at room temperature with an average humidity of 35%. The photocurrent–voltage measurements were conducted using a Keithley 2400 source measuring system. A class A solar simulator (Newport, model 91195A-1000) provided with a 450 W xenon lamp was used as a light source, and its intensity was adjusted using a NREL-calibrated mono-Si solar cell provided with a BF-7 filter to approximately AM 1.5G, 1 sun light intensity. The electrochemical impedance spectra measurements were performed using a frequency response analyzer (Solartron, SI 1260) that was connected to a potentiostat (Solartron 1287) at an amplitude of 10 mV and the open circuit voltage (V_{OC}) under 100 mW $cm^{-2}$of illumination. The film thickness of the GNS-CEs was measured using a surface profiler (P-10, Tencor). Cyclic voltammetric measurements were conducted using a potentiostat (CHI600, CHI instruments) in a three electrode configuration using an acetonitrile containing 0.1 M $LiClO_4$, 5 mM LiI, and 0.5 mM I_2 at the scan rate of 10 mV s^{-1}. A Ag/Ag^+ electrode (0.01 M $AgNO_3$ in acetonitrile) was used as the reference electrode. Pore volumes were estimated using the Brunauer–Emmett–Teller (BET, Sorptomatic 1990) method.

ASSOCIATED CONTENT

Supporting Information

Raman spectroscopy results of GNSs. This material is available free of charge via the Internet at http://pubs.acs.org.

AUTHOR INFORMATION

Corresponding Author

*E-mail: syjang@kookmin.ac.kr. Tel: +82-2-910-5768. Fax: +82-2-910-4415.

Notes

The authors declare no competing financial interest.

ACKNOWLEDGMENTS

The authors gratefully acknowledge support from the Korea Research Council of Fundamental Science & Technology (KRCF) and KIST for 'National Agenda Project (NAP)'

program, and the Basic Science Research Program through the National Research Foundation of Korea (NRF), funded by the Ministry of Education, Science, and Technology (2011-0008698). D.Y.K. acknowledges support from the KIST Institutional Programs (Project 2E22831 and 2K01970).

REFERENCES

(1) Ruoff, R. *Nat. Nanotechnol.* **2008**, *3* (1), 10−11.
(2) Allen, M. J.; Tung, V. C.; Kaner, R. B. *Chem. Rev.* **2009**, *110* (1), 132−145.
(3) Novoselov, K. S.; Geim, A. K.; Morozov, S. V.; Jiang, D.; Zhang, Y.; Dubonos, S. V.; Grigorieva, I. V.; Firsov, A. A. *Science* **2004**, *306* (5696), 666−669.
(4) Novoselov, K. S.; Geim, A. K.; Morozov, S. V.; Jiang, D.; Katsnelson, M. I.; Grigorieva, I. V.; Dubonos, S. V.; Firsov, A. A. *Nature* **2005**, *438* (7065), 197−200.
(5) Gilje, S.; Han, S.; Wang, M.; Wang, K. L.; Kaner, R. B. *Nano Lett.* **2007**, *7* (11), 3394−3398.
(6) Gomez-Navarro, C.; Weitz, R. T.; Bittner, A. M.; Scolari, M.; Mews, A.; Burghard, M.; Kern, K. *Nano Lett.* **2007**, *7* (11), 3499−3503.
(7) Morozov, S. V.; Novoselov, K. S.; Katsnelson, M. I.; Schedin, F.; Elias, D. C.; Jaszczak, J. A.; Geim, A. K. *Phys. Rev. Lett.* **2008**, *100* (1).
(8) Williams, J. R.; DiCarlo, L.; Marcus, C. M. *Science* **2007**, *317* (5838), 638−641.
(9) Eda, G.; Fanchini, G.; Chhowalla, M. *Nat. Nanotech.* **2008**, *3* (5), 270−274.
(10) Robinson, J. T.; Perkins, F. K.; Snow, E. S.; Wei, Z. Q.; Sheehan, P. E. *Nano Lett.* **2008**, *8* (10), 3137−3140.
(11) Fowler, J. D.; Allen, M. J.; Tung, V. C.; Yang, Y.; Kaner, R. B.; Weiller, B. H. *ACS Nano* **2009**, *3* (2), 301−306.
(12) Lu, J.; Drzal, L. T.; Worden, R. M.; Lee, I. *Chem. Mater.* **2007**, *19* (25), 6240−6246.
(13) Lu, C. H.; Yang, H. H.; Zhu, C. L.; Chen, X.; Chen, G. N. *Angew. Chem., Int. Ed.* **2009**, *48* (26), 4785−4787.
(14) Shan, C. S.; Yang, H. F.; Song, J. F.; Han, D. X.; Ivaska, A.; Niu, L. *Anal. Chem.* **2009**, *81* (6), 2378−2382.
(15) Stankovich, S.; Dikin, D. A.; Dommett, G. H. B.; Kohlhaas, K. M.; Zimney, E. J.; Stach, E. A.; Piner, R. D.; Nguyen, S. T.; Ruoff, R. S. *Nature* **2006**, *442*, 282−286.
(16) Zhao, X.; Zhang, Q. H.; Chen, D. J.; Lu, P. *Macromolecules* **2010**, *43* (5), 2357−2363.
(17) Berger, C.; Song, Z. M.; Li, X. B.; Wu, X. S.; Brown, N.; Naud, C.; Mayou, D.; Li, T. B.; Hass, J.; Marchenkov, A. N.; Conrad, E. H.; First, P. N.; de Heer, W. A. *Science* **2006**, *312*, 1191−1196.
(18) Emtsev, K. V.; Bostwick, A.; Horn, K.; Jobst, J.; Kellogg, G. L.; Ley, L.; McChesney, J. L.; Ohta, T.; Reshanov, S. A.; Rohrl, J.; Rotenberg, E.; Schmid, A. K.; Waldmann, D.; Weber, H. B.; Seyller, T. *Nat. Mater.* **2009**, *8* (3), 203−207.
(19) Sutter, P. W.; Flege, J. I.; Sutter, E. A. *Nat. Mater.* **2008**, *7* (5), 406−411.
(20) Kim, K. S.; Zhao, Y.; Jang, H.; Lee, S. Y.; Kim, J. M.; Ahn, J. H.; Kim, P.; Choi, J. Y.; Hong, B. H. *Nature* **2009**, *457*, 706−710.
(21) Li, X. S.; Cai, W. W.; An, J. H.; Kim, S.; Nah, J.; Yang, D. X.; Piner, R.; Velamakanni, A.; Jung, I.; Tutuc, E.; Banerjee, S. K.; Colombo, L.; Ruoff, R. S. *Science* **2009**, *324*, 1312−1314.
(22) Stankovich, S.; Dikin, D. A.; Piner, R. D.; Kohlhaas, K. A.; Kleinhammes, A.; Jia, Y.; Wu, Y.; Nguyen, S. T.; Ruoff, R. S. *Carbon* **2007**, *45* (7), 1558−1565.
(23) Li, D.; Muller, M. B.; Gilje, S.; Kaner, R. B.; Wallace, G. G. *Nat. Nanotech.* **2008**, *3* (2), 101−105.
(24) Si, Y.; Samulski, E. T. *Nano Lett.* **2008**, *8* (6), 1679−1682.
(25) Tung, V. C.; Allen, M. J.; Yang, Y.; Kaner, R. B. *Nat. Nanotechnol.* **2009**, *4* (1), 25−29.
(26) Nakamura, J.; Yoo, E.; Okata, T.; Akita, T.; Kohyama, M.; Honma, I. *Nano Lett.* **2009**, *9* (6), 2255−2259.
(27) Liu, Y.; Qu, L. T.; Baek, J. B.; Dai, L. M. *ACS Nano* **2010**, *4* (3), 1321−1326.
(28) Wang, E. W.; Guo, S. J.; Dong, S. J. *ACS Nano* **2010**, *4* (1), 547−555.
(29) Ruoff, R. S.; Stoller, M. D.; Park, S. J.; Zhu, Y. W.; An, J. H. *Nano Lett.* **2008**, *8* (10), 3498−3502.
(30) Wang, C. Y.; Wang, Y.; Shi, Z. Q.; Huang, Y.; Ma, Y. F.; Chen, M. M.; Chen, Y. S. *J. Phys. Chem. C* **2009**, *113* (30), 13103−13107.
(31) Yang, Q. H.; Lv, W.; Tang, D. M.; He, Y. B.; You, C. H.; Shi, Z. Q.; Chen, X. C.; Chen, C. M.; Hou, P. X.; Liu, C. *ACS Nano* **2009**, *3* (11), 3730−3736.
(32) Honma, I.; Yoo, E.; Kim, J.; Hosono, E.; Zhou, H.; Kudo, T. *Nano Lett.* **2008**, *8* (8), 2277−2282.
(33) Honma, I.; Paek, S. M.; Yoo, E. *Nano Lett.* **2009**, *9* (1), 72−75.
(34) Wallace, G. G.; Wang, C. Y.; Li, D.; Too, C. O. *Chem. Mater.* **2009**, *21* (13), 2604−2606.
(35) O'Regan, B.; Gratzel, M. *Nature* **1991**, *353*, 737−740.
(36) Imoto, K.; Takahashi, K.; Yamaguchi, T.; Komura, T.; Nakamura, J.; Murata, K. *Sol. Energy Mater. Sol. Cells* **2003**, *79* (4), 459−469.
(37) Suzuki, K.; Yamaguchi, M.; Kumagai, M.; Yanagida, S. *Chem. Lett.* **2003**, *32* (1), 28−29.
(38) Hino, T.; Ogawa, Y.; Kuramoto, N. *Carbon* **2006**, *44* (5), 880−887.
(39) Murakami, T. N.; Ito, S.; Wang, Q.; Nazeeruddin, M. K.; Bessho, T.; Cesar, I.; Liska, P.; Humphry-Baker, R.; Comte, P.; Pechy, P.; Gratzel, M. *J. Electrochem . Soc.* **2006**, *153* (12), A2255−A2261.
(40) Chen, J. K.; Li, K. X.; Luo, Y. H.; Guo, X. Z.; Li, D. M.; Deng, M. H.; Huang, S. Q.; Meng, Q. B. *Carbon* **2009**, *47* (11), 2704−2708.
(41) Lee, W. J.; Ramasamy, E.; Lee, D. Y.; Song, J. S. *ACS Appl. Mater. Interfaces* **2009**, *1* (6), 1145−1149.
(42) Han, J.; Kim, H.; Kim, D. Y.; Jo, S. M.; Jang, S. Y. *ACS Nano* **2010**, *4* (6), 3503−3509.
(43) Kavan, L.; Yum, J. H.; Gratzel, M. *ACS Nano* **2010**, *5* (1), 165−172.
(44) Roy-Mayhew, J. D.; Bozym, D. J.; Punckt, C.; Aksay, I. A. *ACS Nano* **2010**, *4* (10), 6203−6211.
(45) Choi, H.; Kim, H.; Hwang, S.; Han, Y.; Jeon, M. *J. Mater. Chem.* **2011**, *21* (21), 7548−7551.
(46) Hong, W.; Xu, Y.; Lu, G.; Li, C.; Shi, G. *Electrochem. Commun.* **2008**, *10* (10), 1555−1558.
(47) Hummers, W. S.; Offeman, R. E. *J. Am. Chem. Soc.* **1958**, *80* (6), 1339.
(48) Gao, W.; Alemany, L. B.; Ci, L. J.; Ajayan, P. M. *Nat. Chem.* **2009**, *1* (5), 403−408.
(49) Kim, J. H.; Nam, K. W.; Ma, S. B.; Kim, K. B. *Carbon* **2006**, *44* (10), 1963−1968.
(50) Rietveld, I. B.; Suganuma, N.; Kobayashi, K.; Yamada, H.; Matsushige, K. *Macro. Mater. Eng.* **2008**, *293* (5), 387−399.
(51) Hauch, A.; Georg, A. *Electrochim. Acta* **2001**, *46* (22), 3457−3466.
(52) Gratzel, M.; Murakami, T. N. *Inorg. Chim. Acta* **2008**, *361* (3), 572−580.
(53) Boschloo, G.; Hagfeldt, A. *Acc. Chem. Res.* **2009**, *42* (11), 1819−1826.
(54) Papageorgiou, N.; Maier, W. F.; Gratzel, M. *J. Electrochem. Soc.* **1997**, *144* (3), 876−884.
(55) Fang, X. M.; Ma, T. L.; Guan, G. Q.; Akiyama, M.; Kida, T.; Abe, E. *J. Electroanal. Chem.* **2004**, *570* (2), 257−263.
(56) Wang, M. K.; Anghel, A. M.; Marsan, B.; Ha, N. L. C.; Pootrakulchote, N.; Zakeeruddin, S. M.; Gratzel, M. *J. Am. Chem. Soc.* **2009**, *131* (44), 15976.
(57) Li, G. R.; Wang, F.; Jiang, Q. W.; Gao, X. P.; Shen, P. W. *Angew. Chem., Int. Ed.* **2010**, *49* (21), 3653−3656.
(58) Popov, A. I.; Geske, D. H. *J. Am. Chem. Soc.* **1958**, *80* (6), 1340−1352.
(59) Nguyen, S. T.; Stankovich, S.; Piner, R. D.; Chen, X. Q.; Wu, N. Q.; Ruoff, R. S. *J. Mater. Chem.* **2006**, *16* (2), 155−158.
(60) Park, S.; An, J.; Potts, J. R.; Velamakanni, A.; Murali, S.; Ruoff, R. S. *Carbon* **2011**, *49* (9), 3019−3023.

(61) Ventrice, C. A.; Yang, D.; Velamakanni, A.; Bozoklu, G.; Park, S.; Stoller, M.; Piner, R. D.; Stankovich, S.; Jung, I.; Field, D. A.; Ruoff, R. S. *Carbon* **2009**, *47* (1), 145−152.
(62) Wallace, G. G.; Chen, H.; Muller, M. B.; Gilmore, K. J.; Li, D. *Adv. Mater.* **2008**, *20* (18), 3557−+.
(63) Banks, C. E.; Davies, T. J.; Wildgoose, G. G.; Compton, R. G. *Chem. Commun.* **2005**, *7*, 829−841.
(64) Trancik, J. E.; Barton, S. C.; Hone, J. *Nano Lett.* **2008**, *8* (4), 982−987.
(65) Jang, B. Z.; Liu, C. G.; Yu, Z. N.; Neff, D.; Zhamu, A. *Nano Lett.* **2010**, *10* (12), 4863−4868.
(66) Yang, S. H.; Qiu, Y. C.; Zhang, X. F. *Phys. Chem. Chem. Phys.* **2011**, *13* (27), 12554−12558.